ELSEVIER

Journal of Electroanalytical Chemistry 426 (1997) 177–184

JOURNAL OF ELECTROANALYTICAL CHEMISTRY

Hydrogen + oxygen recombination and related heat generation in undivided electrolysis cells

Fritz G. Will

Electric Power Research Institute, 3412 Hillview Avenue, Palo Alto, CA 94304, USA

Received 18 March 1996; revised 12 August 1996

Abstract

This paper presents a mathematical analysis that allows the rate of $H_2 + O_2$ recombination and related heat generation in single-compartment electrolysis cells to be calculated as a function of current density and temperature. The analysis employs electrochemical kinetics and gas evolution-enhanced mass transfer theory. Recent calorimetric results of others during the electrolysis of $K_2CO_3 + H_2O$ solutions in the low current density range from 0.5 to 4 mA cm^{-2} are in good agreement with the theoretical predictions. The fraction of O_2 recombining with H_2 decreases significantly with increasing current density. As much as 27% of the O_2 recombines at 0.5 mA cm^{-2}, but only 4% at 100 mA cm^{-2}. It is shown that the heat generated by $H_2 + O_2$ recombination comprises a significant fraction of cell input energy only at low current densities. At 0.5 mA cm^{-2}, heat due to $H_2 + O_2$ recombination is 120%, but it decreases proportionally to $j^{-1.5}$, with values of 18% at 4 mA cm^{-2}, 0.8% at 40 mA cm^{-2} and only 0.03% at 400 mA cm^{-2}. The analysis also predicts quantitatively the observed enhancement of recombination by O_2 gas sparging and its elimination by N_2 sparging. On the basis of their results at low current densities, a group of researchers recently concluded that $H_2 + O_2$ recombination is the source for the 'excess heat' reported by other groups and attributed by some to 'cold fusion'. However, reported excess heat values, ranging from a low of 23% at 14 mA cm^{-2} to a high of 3700% at 6 mA cm^{-2}, are much larger than can be explained by recombination. Whatever the explanation for the large amounts of excess heat reported by various groups, $H_2 + O_2$ recombination must be rejected as a tenable explanation.

Keywords: Hydrogen + oxygen recombination; Heat generation; Undivided electrolysis cell; Mathematical analysis

1. Introduction

Observation of 'excess heat' in heavy water electrolysis using Pd cathodes was first claimed by Fleischmann et al. [1] and attributed to "electrochemically induced nuclear fusion of deuterium". Later, Mills and Kneizys [2] reported excess heat production when electrolyzing light water K_2CO_3 solutions using Ni cathodes and ascribed the excess heat to a nuclear fusion process. Many groups subsequently have reported similar excess heat findings, but the requisite nuclear by-products, commensurate with the excess heat measured, have not been found.

This has prompted a recent study by Jones et al. [3] based on which the authors conclude that $H_2 + O_2$ gas "... recombination can account for most (if not all) currently available reports of excess heat in light water cells". The authors further "... hypothesize that recombination may account for excess heat in similar experiments with Pd electrodes and heavy water".

The present paper examines (1) whether the results of Jones et al. can be explained on the basis of electrode kinetics and mass transfer to gas-evolving electrodes and (2) whether these results, obtained at low current densities, are valid at the much higher current densities generally employed by others in their excess heat findings.

2. Experimental

Only certain features of the electrochemical cell are commented upon here which are of particular interest to the understanding of the results.

Jones et al. [3] used one-compartment glass cells of 2.5 cm diameter and 6 cm length with an electrolyte volume of ca. 16.5 cm^3 and a head space of ca. 1.5 cm^3. A cell modification had provisions for gas sparging through a glass frit at the bottom of the cell. The gases were vented through tubes in the cell screw cap. The anode was a straight Pt wire of 0.6 mm diameter and 3.6 cm submerged length (electrode area 0.7 cm^2). The cathode consisted of (a) a flat 1 cm × 1 cm × 1 mm thickness sintered Ni sheet,

0022-0728/97/$17.00
PII S0022-0728(96)04972-8

spaced about 0.9 cm from the Pt wire or (b) a 2 cm × 1 cm × 1 mm sintered Ni sheet, bent into a semicylinder of ca. 1.3 cm diameter and surrounding the Pt wire cylinder symmetrically at a distance of ca. 0.6 cm. The effective electrode areas in both cases were approximately 2 cm^2, as will be described in Section 5.1.

In a few experiments, one glass tube each (open to the electrolyte on one end) was placed around the anode and cathode to impede gas recombination. For other experiments, O_2 sparging at 1.2 ml min^{-1} or N_2 sparging at 1.7 ml min^{-1} were employed, corresponding to fluxes of 0.32 and 0.45 ml min^{-1} cm^{-2} of cell cross-section.

Cell currents were applied in the range from 1 to 8 mA, corresponding to a gas evolution (H_2 and O_2) rate from 0.01 to 0.08 ml min^{-1}, or about 1/100 of the sparging rate.

The electrolyte was generally 0.6 M K_2CO_3 solution in H_2O and the temperature either 25°C (expt. 1 and 2) or 30.4°C (expt. 3 and 4).

3. Results

The major experimental results of Jones et al. [3] are shown in Table 1. They are grouped differently from those in the original paper, namely (a) results on gas-evolving anode and cathode with no glass tubes surrounding the electrodes and with no additional gas sparging, (b) results like those in case (a) but with glass tubes surrounding anode and cathode, and (c) results like those in case (a) with no tubes but with O_2 or N_2 gas sparging.

In Table 1, I and E are the measured cell current and voltage; $P_{in} = IE$ represents the total electrical power input; P_{meas} is the heat rate, measured with an isothermal differential heat conduction calorimeter; $P_{cell} = I(E - E_{thn})$ is the cell input power if all evolved H_2 and O_2 is vented; $E_{thn} = 1.48$ V is the thermoneutral potential; $P_r = P_{meas} - P_{cell}$ is the heat rate due to $H_2 + O_2$ recombination in the cell (termed excess heat rate by Jones et al); and $q_r = 100P_r/P_{cell}$ is the power due to $H_2 + O_2$ recombination, expressed as a percentage of cell input power.

The accuracy of the entire system for determining P_{meas} is ±0.1 mW in the case of gas sparging and about ±0.08 mW for no gas sparging, as evident from figs. 3 and 4 in Jones et al. [3].

The most significant results can be summarized as follows. At the low currents employed by Jones et al., a significant fraction of excess heat is generated if no measures are taken to prevent $H_2 + O_2$ recombination (expt. 1a to 4b in Table 1). However, the amount of heat decreases appreciably with increasing current, that is from 121.1% at 0.96 mA to 17.8% at 8.08 mA. Gas recombination is essentially prevented (expt. 2a and 2c) if the two electrodes are surrounded by glass tubes; then P_{meas} becomes almost identical to P_{cell}. Sparging with O_2 (no tubes present) increases the fraction of recombined H_2 and O_2 (hence the heat generated) from 105% with no sparging (expt. 2b) to 1049% with O_2 sparging (expt. 3b). N_2 sparging prevents $H_2 + O_2$ recombination (expt. 3a and 4c) or at least greatly impedes it (expt. 4d).

4. Theoretical

4.1. Simultaneous O_2 reduction and H_2 evolution

$H_2 + O_2$ recombination could principally occur either by H_2, evolved at the (Ni) cathode, reacting at the (Pt) anode surface, or O_2, evolved at the anode, reacting at the cathode.

However, it is well established that the rate of H_2 oxidation (gas recombination) on electrodes, such as Pt, Pd and Ni at the potentials of O_2 evolution is negligible [4] due to the inhibiting effect of chemisorbed O or oxides [5,6].

In contrast, O_2 reduction proceeds readily on metal

Table 1
Experimental results by Jones et al. [3]

Expt. no.	I/mA	E/V	P_{in}/mW	P_{meas}/mW	P_{cell}/mW	P_r/mW	q_r/% [a]	Comments
1a	0.96	1.83	1.76	0.74	0.33	0.41	121.1	— [b]
2b	1.04	1.86	1.93	0.80	0.39	0.41	105.1	— [b]
1b	1.66	1.91	3.17	1.27	0.71	0.56	78.5	— [b]
4a	4.17	2.04	8.51	3.86	2.33	1.53	65.4	— [b,c]
4b	8.08	2.61	21.09	10.76	9.13	1.63	17.8	— [c]
2a	1.02	2.09	2.13	0.73	0.62	0.11	17.7	tubes [b,d]
2c	1.01	2.18	2.20	0.66	0.71	−0.05	−5.7	tubes [b,d]
3b	1.08	1.61	1.74	1.61	0.14	1.47	1049	O_2 [b]
3a	1.04	1.84	1.91	0.28	0.37	−0.09	−25.7	N_2 [b]
4c	5.73	2.62	15.01	6.59	6.53	0.06	0.9	N_2 [c]
4d	5.68	2.72	15.45	7.41	7.04	0.37	5.3	N_2 [c]

[a] $q_r = 100P_r/P_{cell}$ is the heat fraction generated by $H_2 + O_2$ recombination.
[b] 1 × 1 cm^2 Ni cathode, planar: ca. 2 cm^2 active area.
[c] 2 × 1 cm^2 Ni cathode, semi-circle: ca. 2 cm^2 active area.
[d] Open-ended glass tubes surround anode and cathode.

surfaces free from chemisorbed oxygen or oxides (hydroxides). At the reversible H_2 evolution potential, the noble metals, including Pd [4], as well as Ag and Ni [7], are oxide-free. On H_2-evolving Pd and Ni cathodes, as used in most 'cold fusion cells', O_2 reduction

$$O_2 + 2H_2O + 2e^- \rightarrow 4OH^- \quad (1)$$

occurs simultaneously to H_2 evolution [4]

$$2H_2O + 2e^- \rightarrow H_2 + 2OH^- \quad (2)$$

The rate of O_2 reduction is controlled by the diffusion of dissolved O_2 to the cathode surface and the two cathodic partial current densities are additive:

$$j = j_r + j_{H_2}, \quad (3)$$

where j, j_r and j_{H_2} are respectively the total (externally measured), O_2 reduction and H_2 evolution currents referred to the cathode area. The rates per unit cathode surface area at which O_2 and H_2 gas are released to the gas phase above the electrolyte are therefore

$$v_{O_2} = V_M(j - j_r)/4F \quad (4)$$

$$v_{H_2} = V_M(j - j_r)/2F = (V_M/2F)j_{H_2} \quad (5)$$

where v_{O_2} and v_{H_2} are the volumes of O_2 and H_2 released per unit time and area respectively; V_M is the molar volume of ideal gases at standard pressure and temperature ($22.41\,mol^{-1}$) and F is the Faraday constant. Thus, while the H_2 evolution current density ($j_{H_2} = j - j_r$) is actually smaller than the O_2 evolution current density ($j_{O_2} = j$), the volumes of H_2 and O_2 released to the gas phase are in stoichiometric proportion ($v_{H_2} = 2v_{O_2}$).

In spite of an *apparent* $H_2 + O_2$ recombination—as would be deduced from the fact that the measured quantities of H_2 and O_2 are smaller than corresponding to Faraday's law—the actual mechanism is not $H_2 + O_2$ recombination but rather the electrochemical reduction of O_2 on the cathode, leading to a correspondingly smaller amount of H_2 generation for a given current.

4.2. Effect of H_2 evolution-enhanced mass transport on the diffusion layer

It has been known for some time that the rate of mass and heat transfer to an electrode is increased by gas evolution on that electrode. Ibl et al. [8] performed detailed experiments [9] on the effect of H_2 evolution on the reduction of Fe^{3+} ions on Pt in 1 M H_2SO_4 and adapted penetration theory [10] to model the experimental results successfully. The theory involves penetration of the diffusion layer, i.e. the replacement of the volume of a gas bubble leaving the surface, by fresh electrolyte.

The latter contains the bulk concentration of dissolved reactant (Fe^{3+}) which decays rapidly according to a non-steady state diffusion process. This process is equivalent to a considerable decrease of the mean diffusion layer thickness compared with that due to natural convection. Ibl et al. [8] derived the expression

$$\delta = \left[\pi rD/6(1 - \Theta)v_{H_2}\right]^{1/2} \quad (6)$$

where r is the bubble radius, D is the diffusivity of dissolved reactant (Fe^{3+}), Θ is the surface fraction covered with bubbles, $v_{H_2}/ml\,cm^{-2}\,s^{-1}$ is the gas (H_2) evolution rate. Assumptions in the derivation of Eq. (6) are that (a) solution with bulk concentration reaches the surface upon bubble release, (b) the reactant reduction is diffusion-controlled, and (c) bubble evolution occurs uniformly across the entire surface. Expressing the H_2 evolution rate in Eq. (6) in terms of j_{H_2} according to Eq. (5) yields

$$\delta = \left[\pi rFD/3(1 - \Theta)V_M j_{H_2}\right]^{1/2} \quad (7)$$

Thus, a straight line with slope -0.5 should result from a log δ vs. log j_{H_2} plot.

Ibl et al. [8] showed that Eq. (7) is obeyed within $\pm 6\%$ for H_2 evolution in acid. However, for H_2 evolution in alkali and for O_2 or Cl_2 evolution, slopes from -0.36 to -0.87 have been observed [11]. Other theoretical models, such as the hydrodynamic model [12] and the micro-convection model [13], predict slopes of -0.33 and -0.48 respectively. Treatment of bubble streams [14] also leads to a slope of -0.5. While no present model is capable of explaining the variety of all experimental findings, all three models predict that δ decreases with increasing gas evolution current to some fractional power, in agreement with the experimental findings.

4.3. Effect of current density on fraction of O_2 recombining

The current density of reactant reduction j_r follows from Fick's law of diffusion

$$j_r = z_r FcD/\delta \quad (8)$$

where z_r is the number of electrons per mole of reactant (4 for O_2), and c is the reactant concentration.

The applied current density j is a direct measure for the total amount of O_2 evolved. The fraction of O_2 recombining, j_r/j, is determined from Eqs. (3), (6) and (7) by eliminating δ and j_{H_2}:

$$j_r/j = b/\left\{2j\left[(1 + 4j/b)^{1/2} - 1\right]\right\} \quad (9)$$

$$b = 48FV_M c^2 D(1 - \Theta)/\pi r \quad (10)$$

Eq. (8) predicts that the fraction of O_2 recombining decreases with increasing current density j. Validity of Eq. (9) assumes that O_2 reduction on the H_2-evolving cathode occurs under diffusion control with $c = 0$ at the cathode surface (limiting diffusion current regime), as has been shown to be true for active noble metals, oxide-free Ni and many other metals [4,7].

4.4. Heat generation by $H_2 + O_2$ recombination

Excess heat is often reported as a fraction of the cell input power, P_{cell}, which, for vented cells with no $H_2 + O_2$ recombination, is

$$P_{cell} = I(E_{cell} - E_{thn}) \quad (11)$$

where I is the cell current, E_{cell} is the cell voltage and E_{thn} is the thermoneutral potential (volt equivalent of the formation enthalpy for H_2O (1.48 V) or D_2O (1.53 V)). Expressing the recombination heat rate $Q_r(P_r)$ as a fraction of the cell input heat $Q_{cell}(P_{cell})$ yields

$$q_r = Q_r/Q_{cell} = P_r/P_{cell} = P_r/I(E_{cell} - E_{thn}) \quad (12)$$

Since

$$P_r = I_r E_{thn} \quad (13)$$

$$q_r = I_r E_{thn}/I(E_{cell} - E_{thn}) \quad (14)$$

E_{cell} is a function of current and can often be approximated by

$$E_{cell} = IR_i + E_o \quad (15)$$

where R_i is the internal cell resistance and E_o is the open circuit voltage. Eliminating E_{cell} from Eqs. (14) and (15) and using current densities yields

$$q_r = j_r/[j(j/j_{thn} + E_o/E_{thn} - 1)] \quad (16)$$

where

$$j_{thn} = I_{thn}/A_{cath} = E_{thn}/R_i A_{cath} \quad (17)$$

is the (hypothetical) current density that would originate if the thermoneutral potential were applied across the specific internal cell resistance (A_{cath} is the cathode area). Combining Eqs. (9) and (16), under elimination of j_r, leads to an expression of the relative excess heat rate as a function of cathodic current density:

$$q_r = \left[(1 + 4j/b)^{1/2} - 1\right] / [(2j/b)(j/j_{thn} + E_o/E_{thn} - 1)] \quad (18)$$

For larger current densities, Eq. (18) can be approximated by

$$q_r \approx j_{thn} b^{1/2}/j^{3/2} \quad (19)$$

This results in an error of less than 10% for $j > 0.015\,A\,cm^{-2}$ in the Jones et al. case of 0.6 M K_2CO_3 at 25°C. When plotting $\log q_r$ versus $\log j$, a straight line should be obtained at moderate to high current densities with a slope of −1.5 and an intercept with the $\log j = 0$ axis at $\log(j_{thn} b^{1/2})$. Excess heat rate due to $H_2 + O_2$ recombination thus decreases steeply with increasing current density. Different electrolytes and temperatures result in a parallel shift of the straight lines in a log–log plot, in accordance with Eq. (19), as b is affected by the changing values of c, D, Θ and r in Eq. (10); but the slope remains −1.5.

5. Discussion

5.1. Comparison of H_2 evolution-enhanced reduction of O_2 and other reactants

Proper discussion and use of the results of Jones et al. [3], as shown in Table 1, requires determining the applied current density j. Two different geometries were used, and the current distributions are not the same in both cases. However, the effective surface areas may be estimated: in the case of a $1 \times 1\,cm^2$ Ni sheet cathode at about 0.9 cm distance from a 3.6 cm long Pt wire anode, the backside of the Ni sheet will receive considerable current, and both sides will be counted, giving approximately $2\,cm^2$ area. In the second case of a $2 \times 1\,cm^2$ Ni sheet bent into a semi-circle at a radial distance of ca. 0.6 cm from the Pt wire in its center, the backside is essentially shielded, and the effective area is also about $2\,cm^2$.

Further discussion in terms of the penetration (or other) model requires determination of the partial current densities of H_2 evolution j_{H_2} and O_2 reduction j_r. The latter is readily determined from Eq. (13), realizing that the heat rate from recombination P_r is related to the measured heat rate P_{meas} by

$$P_r = P_{meas} - P_{cell} \quad (20)$$

Hence

$$j_r = (P_{meas} - P_{cell})/E_{thn} A_{cath} \quad (21)$$

j_{H_2} is readily calculated from Eq. (3). Further, the gas evolution rate and diffusion layer thickness are computed from Eqs. (5) and (7) respectively. The results are summarized in Table 2 for H_2-evolving Ni cathodes in 0.6 M K_2CO_3 without N_2 or O_2 sparging and without the use of glass tubes to mitigate $H_2 + O_2$ recombination. Fig. 1. shows the customary plot of the data of Table 2 in terms of $\log \delta$ vs. $\log j_{H_2}$ according to Eq. (7). Also shown are the results of Ibl et al. [8] (on the reduction of Fe^{3+} in 1 M H_2SO_4 on H_2-evolving smooth and platinized Pt) and of Janssen and Hoogland [11] (on the reduction of Ce^{4+} in 1 M H_2SO_4 and of $Fe(CN)_6^{3-}$ in 1 M KOH on H_2-evolving Pt).

The data points of Jones et al. (with the exception of one point) lie on a straight line with slope of about −0.6. This agrees well with the data of Ibl et al. [8] and Janssen and Hoogland [11] on smooth Pt in acid which give

Table 2
Diffusion layer thickness and $H_2 + O_2$ recombination

Expt. no.	j/mA cm^{-2}	j_r/mA cm^{-2}	j_{H_2}/mA cm^{-2}	δ/mm	f_r/% [a]
1a	0.48	0.137	0.343	394	28.5
2b	0.52	0.138	0.382	391	26.5
1b	0.83	0.189	0.641	286	22.8
4a	2.09	0.515	1.575	105	24.7
4b	4.04	0.549	3.491	98	13.6

[a] $f_r = 100 j_r/j$ is the fraction of total gas recombining.

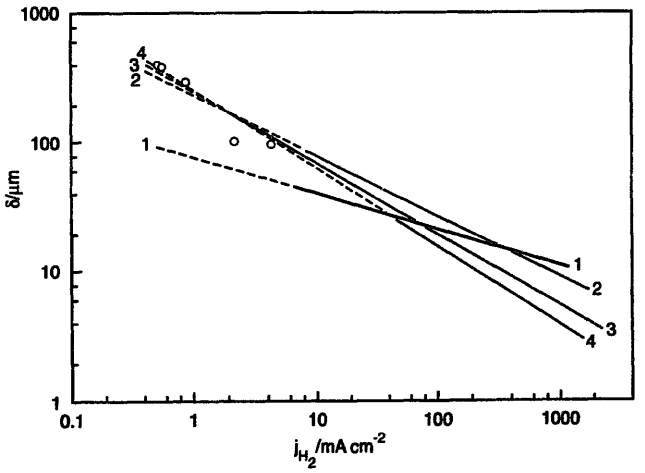

Fig. 1. Diffusion layer thickness vs. current density of H_2 evolution. Data points determined (this study) from calorimetric measurements by Jones et al. [3] on Ni in 0.6 M $K_2CO_3 + O_2$. Solid lines: experimental data of (1) Janssen and Hoogland [11] on Pt in 1 M KOH + 0.03 M $K_3Fe(CN)_6$; (2) Ibl et al. [8] on Pt black in 1 M H_2SO_4 + 0.03 M Fe^{3+}; (3) Ibl et al. [8] on Pt in 1 M H_2SO_4 + 0.03 M Fe^{3+}; (4) Janssen and Hoogland [11] on Pt in 1 M H_2SO_4 + 0.03 M Ce^{4+}. Dotted lines: extrapolated experimental lines.

straight lines with slopes of −0.62 and −0.52 respectively. The Ibl et al. data on Pt black in acid give a straight line with slope −0.46. Extrapolation of these lines to the low current densities employed by Jones et al. shows that the Jones et al. data points fall essentially on those lines. Thus, the results of Jones et al. [3] for O_2 reduction on H_2-evolving Ni in carbonate closely resemble the results of others for the reduction of Fe^{3+} and Ce^{4+} on H_2-evolving Pt in acid. All these results follow the principal behavior (slope close to −0.5) predicted by both penetration and micro-convection theory.

However, the Janssen and Hoogland data on Pt in 1 M KOH yield a straight line of slope −0.36 and quite different values of δ at low current densities. The hydrodynamic model provides a better description of this case, which may be related to the smaller bubble size and the smaller tendency for bubble coalescence in strong alkali.

5.2. Effect of current density on $H_2 + O_2$ recombination

The fraction of O_2 reduced (recombining) at the cathode is predicted by Eq. (9), which has the gas bubble parameter $(1 - \Theta)/r$ entering through b as expressed by Eq. (10). This parameter, while principally accessible to measurement, is not available in the study of Jones et al. [3]. It was therefore determined by fitting the curve predicted by Eq. (9) to the single data point at 4.04 mA cm^{-2}. The curve for 25°C in Fig. 2 for the entire current density range from 0.4 to 1000 mA cm^{-2} was then calculated with Eq. (9), using for c and D the values in H_2O. The values in dilute aqueous solutions, such as 0.6 M K_2CO_3, are, to within a few percent, identical to those in H_2O. Any possible current density dependence of $(1 - \Theta)/r$ was neglected.

With the exception of the data point at 2 mA cm^{-2}, the theoretical curve predicts the observed behavior quite well. At 25°C and low current densities of 0.4 to 0.5 mA cm^{-2}, the predicted and observed $H_2 + O_2$ recombination amounts to 26.5–28.5%. At yet lower current densities, Eq. (9) loses its applicability, and the curves in Fig. 2 should not be extrapolated because the diffusion layer thickness is then determined by natural convection and increases proportionally only to $j_{H_2}^{-0.2}$ rather than $j_{H_2}^{-0.5}$ as predicted by Eq. (7) and used in Eq. (9).

With increasing current density, the predicted fraction of O_2 recombining decreases significantly: 9.7% at 0.01 A cm^{-2}, 4.2% at 0.1 A cm^{-2} and 1.7% at 1 A cm^{-2}.

5.3. Effect of temperature on $H_2 + O_2$ recombination

The effect of temperature on the fraction of O_2 recombining was evaluated by taking into account the temperature-dependence of the O_2 solubility c and diffusivity D (in H_2O) in Eqs. (9) and (10). Any possible temperature-dependence of the gas bubble parameter $(1 - \Theta)/r$ was neglected. Curves for temperatures from 0 to 95°C were thus calculated from Eq. (9) and are shown in Fig. 2. It is seen that $H_2 + O_2$ recombination becomes less significant with increasing temperature. This is due to the fact that j_r/j_{H_2} is proportional to $cD^{1/2}$ and that the decrease of c with increasing temperature outweighs the increase of D as the temperature rises. This effect becomes more pronounced at higher temperatures, as c decreases precipitously when the boiling point of the aqueous solution is approached.

5.4. Effect of gas sparging on $H_2 + O_2$ recombination

Jones et al. [3] conducted experiments on the effect of O_2 and N_2 sparging on the rate of $H_2 + O_2$ recombination in a cell without glass tubes surrounding the electrodes.

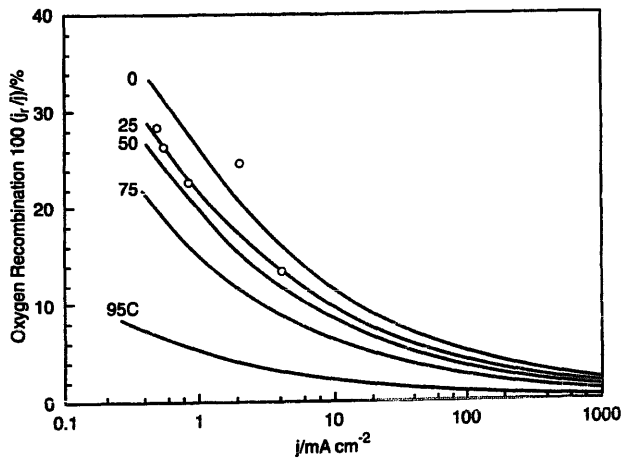

Fig. 2. Predicted percentage of total O_2 recombining at cathode vs. cell current density at different temperatures. Data points determined (this study) from calorimetric measurements by Jones et al. [3].

Table 3
Effect of O_2 and N_2 sparging on $H_2 + O_2$ recombination

Expt. no.	j/ mA cm^{-2}	j_r/ mA cm^{-2}	j_{H_2}/ mA cm^{-2}	v_{sp}/ ml cm^{-2} min^{-1} [a]	Sparging gas	j_{rtheor}/ mA cm^{-2}
2b	0.52	0.138	0.382	0	—	0.144
3b	0.54	0.496	0.044	0.6	O_2	0.56
3a	0.52	−0.032	0.52	0.85	N_2	0.0014

[a] Sparging rate referred to unit area of cathode.

Table 3 shows the results of evaluating the Jones et al. experiments 2b, 3b, and 3a, with no sparging, O_2 sparging at 0.6 ml cm^{-2} min^{-1} and N_2 sparging at 0.85 ml cm^{-2} min^{-1} respectively. These rates are referred to unit cathode area.

The relevant H_2 and O_2 evolution rates were determined from j_r and j_{H_2}, which in turn were computed from the measured heat of recombination (see Table 1) and current, using Eqs. (21) and (3). An H_2 evolution current density of 0.5 mA cm^{-2} corresponds to H_2 and O_2 evolution rates of $v_{H_2} = 0.0036$ ml cm^{-2} min^{-1} and $v_{O_2} = 0.0018$ ml cm^{-2} min^{-1} respectively.

With no sparging and only H_2 and O_2 evolution occurring, the partial pressure of O_2 in the gas head space is

$$p_{O_2} = (1/3)(p_{bar} - p_{H_2O}) \quad (22)$$

where p_{bar} is the barometric pressure and p_{H_2O} is the vapor pressure of H_2O.

With O_2 sparging

$$p_{O_2(O_2sp)} = \left[(v_{O_2sp} + v_{O_2})/v_t\right](p_{bar} - p_{H_2O}) \quad (23a)$$

where

$$v_t = v_{O_2sp} + v_{O_2} + v_{H_2} \quad (23b)$$

With N_2 sparging

$$p_{O_2(N_2sp)} = (v_{O_2}/v_t')(p_{bar} - p_{H_2O}) \quad (24a)$$

where

$$v_t' = v_{N_2sp} + v_{O_2} + v_{H_2} \quad (24b)$$

With no sparging, j_{rtheor} is readily calculated from Eq. (9), using for b the value obtained by fitting the curve to the data point at 4.04 mA cm^{-2} (Fig. 2); the calculated value agrees closely with the experimental value (see Table 3).

With O_2 sparging, the recombination current density is calculated from

$$j_{rO_2sp} = j_r(p_{O_2(O_2sp)}\delta)/(p_{O_2}\delta_{sp}) \quad (25)$$

where δ and δ_{sp} are the diffusion layer thicknesses with electrolysis alone and both electrolysis and sparging respectively; δ is determined from Eq. (7) (see also Fig. 1 and Table 2) as 377 mm. δ_{sp} has been measured as a function of sparging rate in 2 M NaOH by Ibl et al. [8]. Using their data, an approximate value of $\delta_{sp} = 290\ \mu$m was determined for fine-pore glass frits. This leads to a calculated value for j_{rO_2sp} (or j_{rtheor} in Table 3) of 0.56 mA cm^{-2}, in good agreement with the experimental value of 0.496 mA cm^{-2}.

With N_2 sparging, the very small value of $j_{rN_2sp} = 0.0014$ mA cm^{-2} is predicted; experimentally, the small value of −0.032 mA cm^{-2} was determined.

Thus, both the observed increase of $H_2 + O_2$ recombination by O_2 sparging and the observed virtual elimination of recombination by N_2 sparging are readily interpreted. The major factor is the change of the O_2 partial pressure, and hence the O_2 concentration in the electrolyte. The second factor is the change of the diffusion layer thickness which depends upon the rate of gas sparging.

5.5. Heat generated from $H_2 + O_2$ recombination

In contrast to the simple dependency of δ on the H_2 evolution rate (j_{H_2}), the excess heat rate depends on the measured current density j in a more complex form and, furthermore, is affected by electrode spacing and electrode kinetics, such as the O_2 overvoltage. This is expressed in Eqs. (16)–(19) by the presence of the internal resistance R_i and the open circuit voltage E_o. For the case of Jones et al. [3], the experimental current–voltage curve allows determination of $R_i = 107\ \Omega$, equivalent to $j_{thn} = 0.0069$ A cm^{-2} (see Eq. (17)), and $E_o = 1.73$ V. The curve in Fig. 3, representing a plot of $\log q_r$ vs. $\log j$, was computed from Eq. (18). As seen, the theoretical curve predicts the actually observed behavior at lower current densities quite well. No data are available to confirm the predicted behavior at larger current densities, in particular, the straight line with slope −1.5, predicted by Eq. (19) for current densities larger than 0.015 A cm^{-2}.

However, two facts point to the correctness of the predicted behavior at larger current densities. (1) The data obtained by Jones et al. [3] follow closely the simple

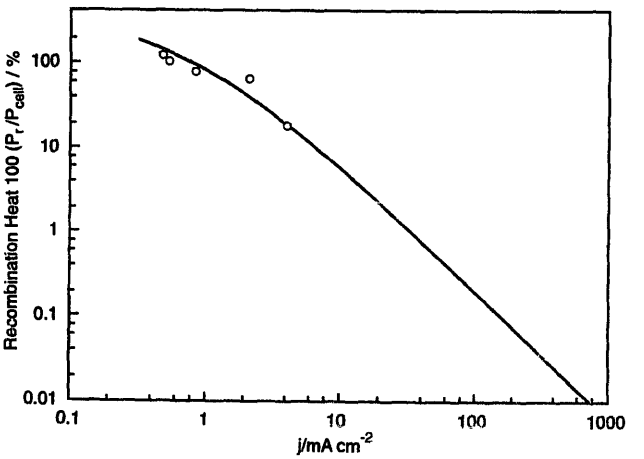

Fig. 3. Predicted heat rate due to $H_2 + O_2$ recombination (as percentage of cell power) vs. cell current density. Data points measured by Jones et al. [3].

straight-line behavior of the log δ vs. log j_{H_2} plot in Fig. 1, both predicted by penetration theory and confirmed by others up to current densities of 1 A cm^{-2}. (2) The predicted log q_r vs. log j curve in Fig. 3 is based on the same theory.

Fig. 3 predicts that the excess heat generated by $H_2 + O_2$ recombination decreases rapidly with increasing cell current density. At 0.01 A cm^{-2}, 0.1 A cm^{-2} and 0.6 A cm^{-2}, the excess heat due to recombination amounts to only 5.4%, 2% and 0.01% respectively.

Similar values are expected for other dilute aqueous electrolyte solutions if the electrode arrangement and anode material are similar to the Jones et al. case. Otherwise, correction has to be made for different internal cell resistance and open circuit voltage. Taking this into account, Fig. 3 predicts approximate values for the excess heat generated by $D_2 + O_2$ recombination in 0.1 M LiOD + D_2O cells.

Fig. 3 and the underlying Eq. (18) are valid only if recombination in the gas head space is prevented by submerging the electrodes fully and protecting the electrode leads with plastic sleeves. It is well established [15] that significant reaction takes place when catalytic electrodes are only partially submerged in the electrolyte.

Gas recombination may also increase significantly when the electrolyte solution boils, as this may lead to parts of the electrode surfaces being exposed to H_2 (D_2) and O_2 which are present in the head space.

5.6. Comparison between predicted and measured $H_2 + O_2$ recombination

With the exception of the study by Jones et al. [3], the author is not aware of other measurements of $H_2 + O_2$ recombination as a function of the current.

However, a few measurements or estimates have been performed at selected currents. Jow et al. [16] found that recombination at 60 or 240 mA cm^{-2} amounted to less than 1%, as determined by weight loss measurements of cells during electrolysis. The present study predicts upper bounds for recombination of 5% and 2.8% at 60 mA cm^{-2} and 240 mA cm^{-2} respectively.

Srinivasan et al. [17] determined gas recombination by collecting the gases formed in 0.6 M K_2CO_3. They obtained less than 10% gas recombination below 40 mA cm^{-2}. The present study predicts less than 5.7% under these conditions.

Lastly, Divisek et al. [18] determined gas recombination from the volume of the $D_2 + O_2$ mixture evolved from a cell with a Pd cathode in 0.1 M LiOD at 547 mA cm^{-2} and 27.6°C. They determined up to 22% recombination in the first 10 min of loading the Pd with D, decreasing to 6% in 180 min. The present study predicts a limit of 2.2% gas recombination under these conditions. The exceptionally high measured values during the first 60 min could be due to the facts that (1) the method employed yielded only the sum of the D occluded by the Pd *and* the D_2 recombining with O_2 and (2) the amount of D occluded was assumed to be identical to that measured on another Pd electrode in a different cell and at a different temperature. Furthermore, no mention was made of any measurements to ascertain the absence of any leaks in the gas collection system. The vital importance of proper procedures in similar gas volume measurements has been emphasized by other authors [19]. A gas leak as small as 0.008 ml s^{-1} would explain the high steady-state value of 6% recombination determined by Divisek et al. [18].

Table 4
Observed excess heat vs. predicted $H_2 + O_2$ recombination heat

Reference	j/mA cm^{-2}	q_{exc}/% [a]	q_r/% [b]
Mills and Kneizys [2]	~6 [c]	156–3766	11
Noninski [20]	~4 [d]	160	18
Notoya and Enyo [21]	10–700	270–340	0 [e]
Srinivasan et al. [17]	14–40 [f]	23–130	0.8–3.3

[a] $q_{exc} = 100 P_{meas} / P_{cell}$.
[b] $q_r = 100 P_r / P_{cell}$.
[c] Average of pulsed current; cathode area ill-defined (jelly role).
[d] Cathode area ill-defined (jelly role).
[e] H_2 sparging eliminates $H_2 + O_2$ recombination.
[f] High-power group of experiments.

5.7. Excess heat claims vs. heat generated by $H_2 + O_2$ recombination

Studies in light water cells aimed at detecting excess heat, have generally employed lower current densities than studies in heavy water cells and are, therefore, more likely to be affected by heat generated from partial $H_2 + O_2$ recombination.

Table 4 summarizes some of the excess heat findings reported in specified current ranges and compares these experimental results with the excess heat for $H_2 + O_2$ recombination predicted in the present study for the Jones cell geometry with $R_i = 107\ \Omega$ and $E_o = 1.73$ V.

It is evident that the reported excess heat values are significantly larger than the heat attributable to $H_2 + O_2$ recombination. Even complete recombination cannot explain the observed results, with the exception of those of Noninski [20]. In another case of reported excess heat, the possibility of recombination is eliminated by employing H_2 sparging [21]. Thus, whatever the explanation for the reported excess heat, it cannot result from $H_2 + O_2$ recombination.

6. Conclusions

The experimental results of Jones et al. [3] on heat generated by $H_2 + O_2$ recombination during electrolysis of 0.6 M $K_2CO_3 + H_2O$ solutions in undivided cells can be predicted by applying gas evolution-enhanced mass trans-

fer theory. However, the results were obtained at small current densities, from 0.5 to 4 mA cm^{-2}; extrapolation of these findings to the much larger current densities, generally employed in 'cold fusion' studies, is not permissible and has led Jones et al. to incorrect conclusions.

$H_2 + O_2$ recombination actually is the electrochemical reduction of dissolved O_2 on the cathode. The fraction of O_2 'recombining' decreases steeply with increasing current density. For $j > 15\,mA\,cm^{-2}$ the decrease is proportional to $j^{-0.4}$. With the exception of one point, the data points of Jones et al. in the measured range from 0.5 to 4 mA cm^{-2} follow the behavior predicted theoretically. At 25°C, $H_2 + O_2$ recombination amounts to 27% at 0.5 mA cm^{-2}, but to only 10%, 4% and 2% at 10 mA cm^{-2}, 100 mA cm^{-2} and 1000 mA cm^{-2} respectively. The fraction of O_2 recombining is proportional to $cD^{1/2}$ and decreases with increasing temperature since the decrease of c outweighs the increase of D.

As further evidence for the validity of applying mass transfer theory, the observed 3.6-fold enhancement of O_2 recombination by O_2 sparging and its virtual elimination by N_2 sparging are both predicted quantitatively.

Extension of the theory to determining the heat due to $H_2 + O_2$ recombination leads to the prediction that the fraction of cell heat due to recombination decreases strongly with increasing current density; the decrease is proportional to $j^{-1.5}$ for $j > 15\,mA\,cm^{-2}$. Again, application of mass transfer theory is validated by the agreement of predicted data with the measurements of Jones et al. in the range from 0.5 to 4 mA cm^{-2}. The heat due to recombination is 120% at 0.5 mA cm^{-2}, but predicted to be only 2% at 100 mA cm^{-2} (11% at 6 mA cm^{-2} and 0.01% at 700 mA cm^{-2}). By contrast, excess heat reported by other groups at current densities from 6 to 700 mA cm^{-2} is from 23 to 3700%. It is concluded that heat generated by $H_2 + O_2$ recombination must be ruled out as an explanation for the excess heat reported by a number of groups in both light and heavy water electrolysis and sometimes attributed to cold fusion. The question: "what effects (or artifacts) give rise to the excess heat findings?" must therefore still be regarded as unresolved.

References

[1] M. Fleischmann, S. Pons and M. Hawkins, J. Electroanal. Chem., 261 (1989) 301; err. 263 (1989) 187.
[2] R.L. Mills and S.P. Kneizys, Fusion Technol., 20 (1991) 65.
[3] J.E. Jones, L.D. Hansen, S.E. Jones, D.S. Shelton and J.M. Thorne, J. Phys. Chem., 99 (1995) 6973.
[4] M.W. Breiter, Electrochemical Processes in Fuel Cells, Springer, Berlin, 1969, pp. 106, 187, 201.
[5] F.G. Will and C.A. Knorr, Z. Elektrochem., 64 (1960) 258.
[6] F.G. Will and C.A. Knorr, Z. Elektrochem., 64 (1960) 270.
[7] G. Lin-In, N.A. Shumilova, V.S. Bagotsky and P.F. Belmer, Elektrokhimya, 3 (1967) 1279.
[8] N. Ibl, E. Adam, J. Venczel and E. Schalch, Chem. Ing. Tech., 43 (1971) 202.
[9] J. Venczel, Ph.D. Thesis, ETH Zürich, Prom. #3019, 1961.
[10] C.O. Bennett and J.E. Myers, Momentum, Heat and Mass Transfer, McGraw Hill, New York, 1962, p. 489.
[11] L.J.J. Janssen and J.G. Hoogland, Electrochim. Acta, 18 (1973) 543.
[12] L.J.J. Janssen and E. Barendrecht, Electrochim. Acta, 18 (1973) 693.
[13] K. Stephan and H. Vogt, Electrochim. Acta, 24 (1979) 11.
[14] G.M. Whitney and C.W. Tobias, AICHE J., 34 (1988) 1981.
[15] F.G. Will, J. Electrochem. Soc., 110 (1963) 145.
[16] T.R. Jow, E. Plichta, C. Walker, S. Slane and S. Gilman, J. Electrochem. Soc., 137 (1990) 2473.
[17] M. Srinivasan, A. Shyam, T.K. Sankaranarayanan, M.B. Bajpai, H. Ramamurthy, U.K. Mukherjee, M.S. Krishnan, M.G. Nayar and Y.P. Naik, in H. Ikegami (Ed.), Nagoya Conf. Proc. Frontiers of Cold Fusion, Universal Academy Press, Tokyo, 1993, pp. 123–138.
[18] J. Divisek, L. Fürst and J. Balej, J. Electroanal. Chem., 278 (1990) 99.
[19] F.G. Will, K. Cedzynska and D.C. Linton, J. Electroanal. Chem., 360 (1993) 161.
[20] V.C. Noninski, Fusion Technol., 21 (1992) 163.
[21] R. Notoya and M. Enyo, in H. Ikegami (Ed.), Nagoya Conf. Proc. Frontiers of Cold Fusion, Universal Academy Press, Tokyo, 1993, pp. 421–426.